Electronic Supplementary Information

Ligase Amplification Reaction-Catalyzed Assembly of Single Quantum Dot-Based Nanosensor for Sensitive Detection of Alkaline Phosphatase

Fei Ma,‡ Meng Liu,‡ Chun-yang Zhang*

College of Chemistry, Chemical Engineering and Materials Science, Collaborative Innovation Center of Functionalized Probes for Chemical Imaging in Universities of Shandong, Key Laboratory of Molecular and Nano Probes, Ministry of Education, Shandong Provincial Key Laboratory of Clean Production of Fine Chemicals, Shandong Normal University, Jinan 250014, China.

* Correspondence author. Tel.: +86 0531-86186033; Fax: +86 0531-82615258. E-mail: cyzhang@sdnu.edu.cn.

‡ These authors contributed equally.

EXPERIMENTAL SECTION

Chemicals and Materials. All oligonucleotides (Table S1) were synthesized by Sangon Biotech Co., Ltd. (Shanghai, China). Alkaline Phosphatase (ALP), Hhal Methyltransferase (Hhal), bovine serum albumin (BSA) and 10× CutSmart® Buffer were obtained from New England Biolabs (Ipswich, MA, USA). Ampligase® thermostable DNA ligase and its 10× reaction buffer were purchased from Epicentre Biotechnologies (Madison, WI, USA). Thymine DNA Glycosylase (TDG) was bought from R&D System (Minneapolis, MN, USA). The streptavidin-conjugated CdSe/ZnS QDs with a maximum emission of 605 nm (Qdot 605 ITK) were obtained from Invitrogen Corporation (California, USA). The GOX and Na_3VO_4 were obtained from Sigma-Aldrich (St. Louis, MO, USA). All other reagents were of analytical grade and used as received without further purification. Ultrapure water obtained from a Millipore filtration system (Temecula, CA, USA) was used throughout all experiments.

Table S1. Sequences of the Oligonucleotides [a]

note	sequences (5'−3')
detection probe	ATC GAG TGC ACC TGA CTC CTG-P
assistant probe	P-GGA GAA GTC TGC CGT ATC GAG
template	ACG GCA GAC TTC TCC CAG GAG TCA GGT GCA
biotinylated probe	P-CAG GAG TCA GGT GCA-biotin
Cy5-labeled probe	Cy5-ACG GCA GAC TTC TCC

[a] The "P" denotes the phosphate group.

ALP Detection. To perform the dephosphorylation of detection probes, 20 μL of reaction system containing 2 μL of various-concentration ALP, 0.15 μL of 10 μM detection probe, 2 μL of 10× CutSmart® Buffer (500 mM potassium acetate, 200 mM Tris-acetate, 100 mM magnesium acetate, 1000 μg/mL BSA, pH 7.9) was incubated at 37 °C for 30 min, and the reaction was terminated by heating at 65 °C for 5 min. Then the dephosphorylation reaction products were mixed with 0.15 μL of 5 μM assistant probe, 0.15 μL of 5 μM DNA template, 1.2 μL of 5 μM biotinylated probe, 1.2 μL of 5 μM Cy5-labeled probe, 3 μL of ampligase, 10× reaction buffer (200 mM Tris-HCl, pH 8.3, 250 mM KCl, 100 mM $MgCl_2$, 5 mM NAD, and 0.1% Triton® X-100), and 10 U of Ampligase® DNA ligase, with the reaction volume being adjusted to 30 μL. The ligation reaction was carried out for 80 cycles at 95 °C for 1 min, at 58 °C for 2 min. Finally, the ligation products were mixed with 8.3 nM 605QDs in 60 μL of buffer (1.5 mM $MgCl_2$, 50 mM Tris-HCl, 5 mM $(NH_4)_2SO_4$, pH 8.0) for 10 min to form the 605QD/Cy5 Nanoassemblies at room temperature.

Ensemble Fluorescence Measurement. The 50 μL of reaction products was measured using a 1-cm path length quartz cuvette on a Hitachi F-7000 fluorescence spectrophotometer (Tokyo, Japan). The excitation wavelength was 488 nm, and the emission spectra were recorded over the wavelength range of 500 - 720 nm with a slit width of 5 nm for both excitation and emission.

Single-Molecule Detection and Data Analysis. The reaction products were diluted 100-fold in the imaging buffer (1 mg/mL glucose oxidase, 0.4% (w/v) D-glucose, 0.04% mg/mL catalase, 50 μg/mL BSA, 67 mM glycine-KOH, 1 mg/mL trolox, 2.5 mM $MgCl_2$, pH 9.4). For TIRF imaging, 10 μL of samples was directly pipetted to the coverslips. A sapphire 488 nm laser (50 mW, Coherent, USA) was used to excite the 605QDs. The photons from the 605QD and Cy5 were collected by a 100× objective (Olympus, Japan) and imaged with an exposure time of 500 ms by

an Andor Ixon DU897 EMCCD. A region of interest (900 × 900 pixels) of the images was selected for Cy5 molecule counting by using Image J software.

Gel Electrophoresis. The products of ligase amplification reaction were analyzed with 12% desaturating polyacrylamide gel electrophoresis (PAGE) in 1× TBE buffer (9 mM Tris-HCl, pH 7.9, 9 mM boric acid, 0.2 mM EDTA) at a 120 V constant voltage for 50 min at room temperature. The gel was stained with a silver staining kit (81104-1000, Tiandz Inc., Beijing, China) and analyzed by a Bio-Rad ChemiDoc MP Imaging System (Hercules, CA, USA).

ALP Inhibition Assay. For the ALP inhibition assay, 2 μL of Na_3VO_4 with different concentrations was mixed with 2 μL of 1 U/mL ALP at 37 °C for 20 min, respectively. Then, 2 μL of 10× CutSmart® Buffer (500 mM potassium acetate, 200 mM Tris-acetate, 100 mM magnesium acetate, 1000 μg/mL BSA, pH 7.9) and 0.15 μL of 10 μM detection probe was added into the mixture, with the final volume being adjusted to 20 μL. The ALP detection follows the procedures described above.

Preparation of Cell Extracts. Human breast cancer cells (MCF-7 cells) and human embryonic kidney cells (HEK293T cells) were cultured in Dulbecco's modified Eagle's medium (DMEM, Life Technologies, USA) with 10% fetal bovine serum (FBS; Life Technologies, USA) and 1 % penicillin-streptomycin (Gibco, USA) in 5% CO_2 incubator at 37 °C. For real sample analysis, cells were collected with trypsinization and counted by using Countstar BioTech Automated Cell Counter IC1000 (Shanghai, China), washed twice with the ice-cold PBS (pH 7.4, Gibco, USA), and centrifuged at 1,000 rpm for 5 min. Then the cells were suspended in 50 μL of lysis buffer (10 mM Tris-HCl, pH 8.0, 150 mM NaCl, 1% NP-40, 0.25 mM sodium deoxycholate, 1.0% glycerol, and 0.1 mM 4-(2-aminoethyl) benzenesulfonyl fluoride hydrochloride), incubated on ice for 30

min, and then centrifuged at 12,000 rpm for 20 min at 4 °C. The supernatant was transferred into a fresh tube and stored at −80 °C. The protein concentration was measured using a NanoDrop 2000c Spectrophotometer (Thermo Scientific, Wilmington, Delaware, USA).

SUPPLEMENTARY RESULTS

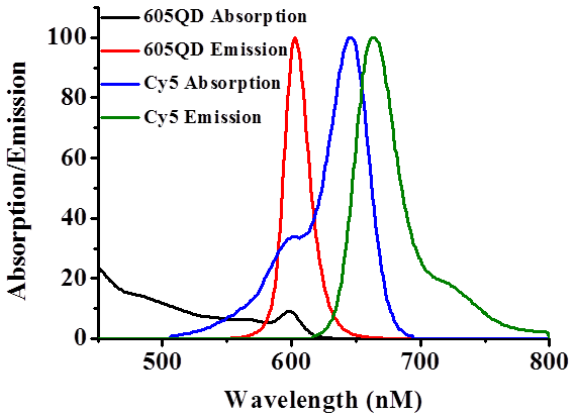

Fig. S1 Normalized absorption and emission spectra of 605QD and Cy5. There is almost no overlap between the 605QD emission (red line) and the Cy5 emission (green line), but there is large spectral overlap between the 605QD emission (red line) and the Cy5 absorption (blue line), indicating that the 605QD and Cy5 can function as the energy donor and the energy acceptor, respectively, to build the efficient FRET system.

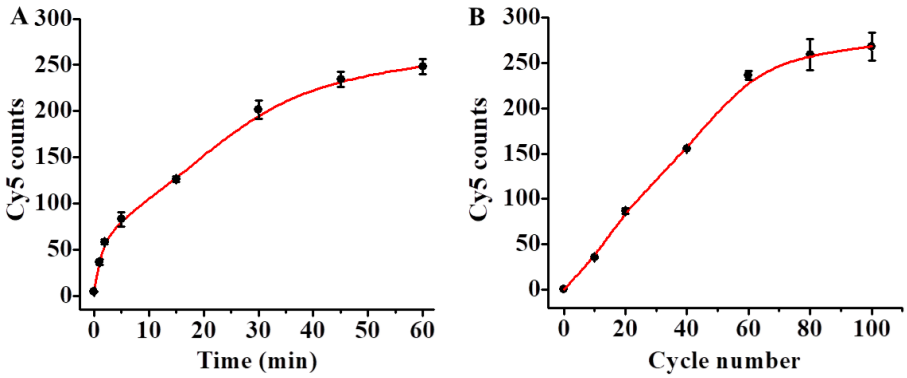

Fig. S2 Variance of Cy5 counts with the ALP incubation time (A) and the cycle number of ligase amplification reaction (B). The ALP concentration is 0.1 U/mL. Error bars represent the standard deviation of three experiments.

To achieve the best assay performance, various experimental parameters including the ALP incubation time and the cycle number of ligase amplification reaction are optimized. As shown in Fig. S2A, the Cy5 counts enhance with the ALP incubation time from 0 to 50 min, and level off beyond 50 min. This may be explained by either the complete loss of ALP activity or the consumption of all available detection probes after 50-min reaction. We also investigated the influence of the cycle number of ligase amplification reaction on the assay performance. As shown in Fig. S2B, the Cy5 counts increase with the cycle number from 0 to 80, and level off beyond 80. This may be explained by the consumption of all available biotinylated probes and Cy5-labeled probes. To reduce the assay time, the incubation time of 50 min and the cycle number of 80 are used in the subsequent researches.

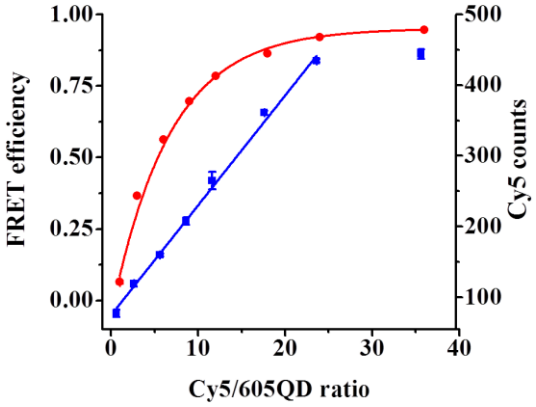

Fig. S3 Variance of FRET efficiency (red color) and Cy5 counts (blue color) with the Cy5-to-605QD ratio. Error bars represent the standard deviation of three experiments.

To investigate the influence of the Cy5-to-605QD ratio upon the assay performance, varied concentrations of Cy5-labeled signal probes were mixed with a fixed concentration of 605QDs (8 nM) to obtain the 605QD/signal probe/Cy5 nanostructure with different Cy5-to-605QD ratio, and the fluorescence intensities of both 605QDs and Cy5 at the excitation wavelength of 488 nm were measured. The FRET efficiency (E) is calculated based on the equation: E (%) = $(1 - F_{ALP}/F_0) \times 100$, where F_{ALP} is the fluorescence intensity of 605QD in the presence of ALP and F_0 is fluorescence intensity of 605QD in the absence of ALP. The obtained FRET efficiency (%) and Cy5 counts are plotted against the Cy5-to-605QD ratio. As shown in Fig. S3 (red color), the FRET efficiency enhances with the increasing Cy5-to-605QD ratio from 1 to 24, and reaches a plateau beyond the ratio of 24, indicating that the assembly of multiple Cy5-labeled signal probes on the surface of a single 605QD can lead to significant improvement of FRET efficiency. Moreover, the Cy5 counts exhibit a linear relationship with the Cy5-to-605QD ratio from 1 to 24 (Fig. S3, blue color), and reach a plateau beyond the ratio of 24. Therefore, the Cy5-to-605QD ratio of 24 is used in the subsequent researches.

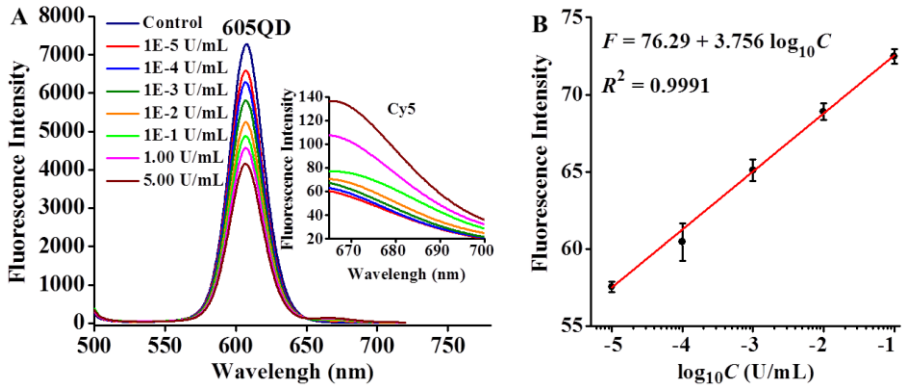

Fig. S4 (A) Measurement of 605QD and Cy5 fluorescence intensity in response to different concentrations of ALP. (B) Linear relationship between the Cy5 fluorescence intensity and the logarithm of ALP concentration in the range from 1×10^{-5} to 0.1 U/mL. Error bars represent the standard deviation of three experiments.

We investigated the sensitivity of the ensemble fluorescence measurement. As shown in Fig. S4A, the 605QD fluorescence intensity decreases with the increasing concentration of ALP, accompanied by the increase of Cy5 fluorescence intensity, suggesting the target-induced efficient FRET between the 605QD and Cy5. Moreover, the Cy5 fluorescence intensity is linearly correlated with the logarithm of ALP concentration in the range from 1×10^{-5} to 0.1 U/mL with a correlation coefficient (R^2) of 0.9991 (Fig. S4B). The regression equation is $F = 76.29 + 3.756 \log_{10} C$, where F is the Cy5 fluorescence intensity and C is the ALP concentration (U/mL). The detection limit is determined to be 1.41×10^{-6} U/mL.

Table S2. Raw data of Fig. 3

Cy5 counts / ALP (U/mL)	sample 1	sample 2	sample 3	mean	SD
0	6	7	7	6.667	0.5773
1×10^{-6}	49	63	57	56.33	7.023
1×10^{-5}	92	96	96	94.67	2.309
1×10^{-4}	123	129	132	128.0	4.583
1×10^{-3}	163	167	170	166.7	3.512
1×10^{-2}	207	207	199	204.3	4.619
0.1	239	256	245	246.7	8.622
0.5	331	329	343	334.3	7.572
1	375	389	413	392.3	19.22
2	471	470	489	476.7	10.69

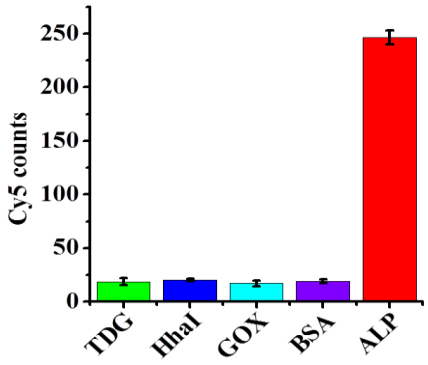

Fig. S5 Measurement of Cy5 counts in response to TDG (0.1 U/mL), HhaI (0.1 U/mL), GOX (50 nM), BSA (50 nM), and ALP (0.1 U/mL), respectively. Error bars represent the standard deviation of three experiments.

To investigate the specificity of the proposed nanosensor, we measured the Cy5 signal in response to the interferences including thymine DNA glycosylase (TDG), HhaI restriction terminionuclease (HhaI), glucose oxidase (GOX), and bovine serum albumin (BSA). TDG can remove thymine moieties from G/T mismatches.[1] HhaI can cleave the double-stranded DNA with the sequence of 5'-GCGC-3'.[2] GOX can catalyse the oxidation of glucose to hydrogen peroxide and D-glucono-δ-lactone.[3] BSA is a frequently used irrelevant protein. Theoretically, none of TDG, HhaI, GOX and BSA can induce dephosphorylation of detection probes to catalyze the assembly of the 605QD/signal probe/Cy5 nanostructure, and thus no Cy5 signal can be detected. As shown in Fig. S5, a high Cy5 signal is detected in response to target ALP, while an extremely low Cy5 signal is observed in response to TDG, HhaI, GOX, and BSA, respectively. The signal of ALP is 13.22-, 12.13-, 14.41-, and 13.16-fold higher than that of TDG, HhaI, GOX and BSA, respectively. The high specificity of the proposed nanosensor can be ascribed to the use of high-fidelity ligase for target ALP recognition and signal conversion.

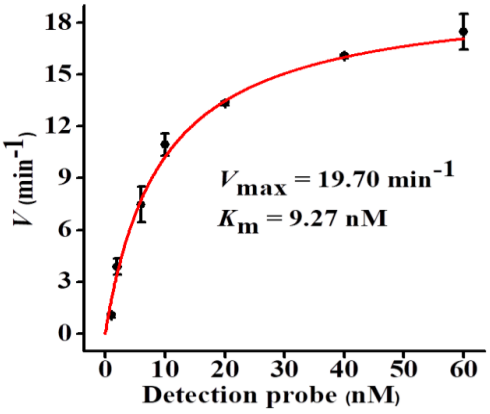

Fig. S6 Analysis of Michaelis−Menten kinetic parameters by the initial-rate method. The ALP concentration is 0.01 U/mL. The ALP incubation time is 5 min. Error bars represent the standard deviation of three experiments.

To investigate the feasibility of the proposed nanosensor for kinetic analysis, the initial velocity (V) in response to different concentrations of detection probes were measured and fitted to the Michaelis–Menten equation $V = V_{max}[S]/(K_m + [S])$, where V_{max} is the maximum initial velocity, and $[S]$ is the concentration of detection probe, and K_m is the Michaelis–Menten constant. As shown in Fig. S6, the initial velocity enhances with the increasing concentration of detection probe from 1 to 60 nM. The V_{max} is determined to be 19.70 min^{-1}, and the K_m is calculated to be 9.27 nM. These results demonstrate that the proposed nanosensor can be used for ALP kinetic analysis.

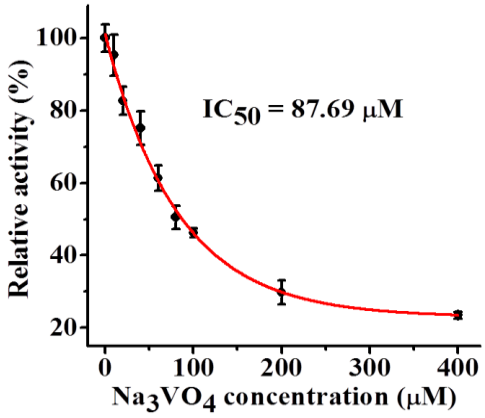

Fig. S7 Variance of the reactive activity of ALP in response to different concentrations of Na_3VO_4. The ALP concentration is 0.1 U/mL. Error bars represent the standard deviation of three experiments.

ALP inhibitors are potential drugs for disease therapy (e.g., the suppression of vascular smooth muscle cell calcification[4] and the treatment of cardiovascular disease[5]). We used a well-known ALP inhibitor sodium orthovanadate[6] (NA_3VO_4) to demonstrate the capability of the proposed nanosensor for ALP inhibition assay. As shown in Fig. S7, the relative activity of ALP decreases

with the increasing concentration of NA_3VO_4 in a dose dependent manner. The IC_{50}, which represents the concentration of inhibitor required to reduce the ALP activity by 50%, is determined to be 87.69 μM, which is similar to the value obtained by using the near-infrared fluorescent probe (141.9 μM).[7] This result suggests that the proposed nanosensor can be used for the screening of ALP inhibitors, holding great potential in drug development.

REFERENCES

1. P. Neddermann, P. Gallinari, T. Lettieri, D. Schmid, O. Truong, J. J. Hsuan, K. Wiebauer and J. Jiricny, *J. Biol. Chem.*, 1996, **271**, 12767-12774.
2. R. J. Roberts, P. A. Myers, A. Morrison and K. Murray, *J. Mol. Biol.*, 1976, **103**, 199-208.
3. R. Wilson and A. P. F. Turner, *Biosens. Bioelectron.*, 1992, **7**, 165-185.
4. S. Narisawa, D. Harmey, M. C. Yadav, W. C. O'Neill, M. F. Hoylaerts and J. L. Millán, *J. Bone Miner. Res.*, 2007, **22**, 1700-1710.
5. M. Haarhaus, V. Brandenburg, K. Kalantar-Zadeh, P. Stenvinkel and P. Magnusson, *Nat. Rev. Nephrol.*, 2017, **13**, 429.
6. U. Sanzhaeva, X. Xu, P. Guggilapu, M. Tseytlin, V. V. Khramtsov and B. Driesschaert, *Angew. Chem.*, 2018, **130**, 11875-11879.
7. S.-J. Li, C.-Y. Li, Y.-F. Li, J. Fei, P. Wu, B. Yang, J. Ou-Yang and S.-X. Nie, *Anal. Chem.*, 2017, **89**, 6854-6860.